PERGAMON

International Journal of Solids and Structures 40 (2003) 6799–6812

INTERNATIONAL JOURNAL OF SOLIDS and STRUCTURES

www.elsevier.com/locate/ijsolstr

A coupled electromechanical analysis of a piezoelectric layer bonded to an elastic substrate: Part II, numerical solution and applications

Benniu Zhang [a], Junqian Zhang [b,*], Jinghong Fan [a]

[a] *Research Center for Materials Mechanics, Chongqing University, Chongqing 400044, China*

[b] *Shanghai Institute of Applied Mathematics and Mechanics, Shanghai University, Shanghai 200072, China*

Received 23 December 2002; received in revised form 15 May 2003

Abstract

This two-part contribution presents a novel and efficient method to analyze the two-dimensional (2-D) electromechanical fields of a piezoelectric layer bonded to an elastic substrate, which takes into account the fully coupled electric and mechanical behaviors. In Part I, we have obtained a system of governing integro-differential equations for the structure via a variational principle. This part presents a numerical solution algorithm of the integro-differential equations and the numerical results of some applications. A numerical algorithm for solving the system of four integro-differential equations with strongly singular kernels is developed. The convergence of the numerical algorithm is discussed. The numerical results suggest that the fully coupled electromechanical analysis is helpful for a better understanding of the performance of the piezoelectric sensor and actuator. The interfacial normal stress is much higher than the interfacial shear stress, suggesting that the interfacial normal stress causes a delamination initiation.

1. Introduction

Piezoelectric materials have been widely used in transducer and actuator industry because of their particular characters. The mostly often-used materials are quartz and piezoceramic (Benes et al., 1995; Wang and Chen, 2000). The latter, which can be used not only as a sensor but also as an actuator (Wang and Chen, 2000; Pal et al., 2000), has an extensive application potential. Bonding of thin piezoceramic layers on an elastic substrate as either an actuator or a sensor is one of the applications. The relationships between the input quantities and the output quantities need to be determined. The stress conditions will be very important in analyzing the structure reliability and integrity. In Part I, we obtained a system of governing integro-differential equations for a piezoelectric layer bonded to an elastic substrate. However, the system of integro-differential equations involves not only high-order derivatives but also integrals with

* Corresponding author. Tel.: +86-21-56338301; fax: +86-21-36033287.
E-mail address: jqzhang@mail.shu.edu.cn (J. Zhang).

0020-7683/$ - see front matter © 2003 Elsevier Ltd. All rights reserved.
doi:10.1016/S0020-7683(03)00312-3

strongly singular kernels. There has not been an algorithm to treat such conditions yet, and a special solution algorithm should be developed to solve the equations.

Integral equations with strongly singular kernels are usually met in solving real world problems (Erdogan and Gupta, 1972; Sankar et al., 1982; Bland, 1970; Plotkin and Dodbele, 1988; Dragos, 1990; Cess and Tiwari, 1969). Muskhelishvili (1953) is the pioneer who discussed systematically the mathematical apparatus of Cauchy type integrals and singular integral equations. Literatures continued to discuss numerical solutions of integro-differential equations with Cauchy singular kernels or weaken kernels (Delves and Walsh, 1974; Loakimidis, 1983; Frankel, 1995). To meet severe singular kernels, Kaya and Erdogan (1987) proposed some formulas to evaluate the integrals having a singularity of the form $(t-x)^{-m}$, $m \geqslant 1$. Using their technique, the severe singular kernels could be weakened at first. Then, it was assumed that an unknown function in the integrals could be replaced by the product of a non-singular part and a pre-estimated singular part. The non-singular part could be approximated by a truncated series of Cheybyshev polynomials. Nevertheless, the algorithm cannot treat the integrals and the derivatives at the same time.

The finite difference method (Lapidus and Pinder, 1982; Li et al., 1999) is often used in solving differential equations. Styś and Styś (2000) introduced a finite difference algorithm to approximate the integro-differential equations without a singular kernel. In our integro-differential equations, we need consider not only the high-order derivatives but also integrals having the strongly singular kernels. After using the technique of Kaya and Erdogan (1987) to weaken the singular kernels, we introduce a quadrature algorithm for the integrals. Subsequently, a finite difference scheme is adopted to deal with the derivatives in the equations. When both the quadrature and the finite difference make use of the same discrete points, the equations result in a system of algebra equations. The contents of the paper will be arranged in the following order. First we introduce a synthesized algorithm for solving the four integro-differential equations with strongly singular kernels. Then the convergence of the numerical algorithm is discussed. Finally the numerical results for applications of piezoelectric layer as an actuator and a sensor are presented.

2. Solution of the governing integro-differential equations

In Part I, the governing integro-differential equations for the coupled electromechanical problem that a piezoelectric layer of thickness, h, with the poling direction parallel to z-axis is bonded to a half-infinite elastic substrate, have been derived as

$$T_{11}N'''' + T_{12}M'''' + T_{13}N'' + T_{14}M'' + T_{15}D_1' + T_{16}D_0' + T_{17}N + T_{18}M + \int_{-l}^{l} \frac{N'(\xi)}{x-\xi}\,\mathrm{d}\xi = \frac{\pi Y^{(s)}}{2(1-v^{(s)2})}\left(\varepsilon_x^{\infty} + \frac{\phi_{bl}b_{31}}{h\delta_{33}}\right), \tag{1}$$

$$T_{21}N'''' + T_{22}M'''' + T_{23}N'' + T_{24}M'' + T_{25}D_0' + T_{26}M + \int_{-l}^{l} \frac{hN''(\xi) - 2M''(\xi)}{(x-\xi)^2}\,\mathrm{d}\xi = 0, \tag{2}$$

$$\delta_{11}hD_0 - \frac{h^3\delta_{33}}{12}D_0'' - (b_{15}+b_{31})M' + \frac{b_{15}h}{2}N' + \frac{b_{33}h^2}{10}M''' - \frac{b_{33}h^3}{24}N''' = 0, \tag{3}$$

$$-120\delta_{11}D_1 + 2h^2\delta_{33}D_1'' - 60b_{15}N' + h^2b_{33}N''' = 0, \tag{4}$$

where the four unknown functions N, M, D_0 and D_1 of the piezoelectric layer are the axial force, the moment, the average and the first moment of the x-component electric displacement. The superscript expresses a derivative with respect to the variable x or ξ. The mechanical boundary conditions read as

$$N(\pm l) = 0, \quad M(\pm l) = 0, \tag{5a,b}$$

$$N'(\pm l) = 0, \quad M'(\pm l) = 0, \tag{6a,b}$$

while the electric boundary conditions on the edges are

$$D_0(\pm l) = 0, \quad D_1(\pm l) = 0. \tag{7a,b}$$

The potential difference, ϕ_{bt}, between the top and bottom surfaces coated with electrodes is given by either

$$\phi_{\mathrm{bt}} = V, \tag{8a}$$

or

$$\phi_{\mathrm{bt}} = \frac{b_{31}}{2l}\int_{-l}^{l} N(\xi)\,\mathrm{d}\xi. \tag{8b}$$

Eq. (8a) represents the case that the prescribed voltage is applied to the piezoelectric layer (actuator). In contrast, Eq. (8b) applies for the case that the piezoelectric layer is used as a sensor along with an open circuit condition which implies that there is no the total free electric charge on the electrodes.

Here the boundary value problem governed by Eqs. (1)–(7b) along with either Eq. (8a) or (8b) is solved numerically by using the method that synthesizes the finite difference and numerical quadrature schemes. The length of the piezoelectric layer is divided into n-segments of length t with $(n+1)$ discrete points x_i $(i = 0, 1, \ldots, n)$ such that

$$t = \frac{2l}{n}, \quad x_i = it - l \ \ (i = 0, 1, \ldots, n). \tag{9a,b}$$

For convenience we introduce the notation $F_i = F(x_i)$ $(i = 0, 1, \ldots, n)$ where F could be any one of M, N, D_0 and D_1 as well as their derivatives. The boundary conditions equations (5a,b) and (7a,b) read as

$$N_0 = 0, \quad M_0 = 0, \tag{10a,b}$$

$$N_n = 0, \quad M_n = 0, \tag{11a,b}$$

$$D_{0,0} = 0, \quad D_{1,0} = 0, \tag{12a,b}$$

$$D_{0,n} = 0, \quad D_{1,n} = 0, \tag{13a,b}$$

while the boundary conditions equations (6a,b) along with the finite difference scheme given in Appendix A leads to four linear algebra equations as follows:

$$-N_2 + 4N_1 - 3N_0 = 0, \quad -M_2 + 4M_1 - 3M_0 = 0, \tag{14a,b}$$

$$-N_{n-2} + 4N_{n-1} - 3N_n = 0, \quad -M_{n-2} + 4M_{n-1} - 3M_n = 0. \tag{15a,b}$$

The governing equations (1) and (2) could be satisfied at the $(n-3)$ discrete points x_i $(i = 2, 3, \ldots, n-2)$ within the interval of $(-l, l)$, i.e.

$$T_{11}N_i'''' + T_{12}M_i'''' + T_{13}N_i'' + T_{14}M_i'' + T_{15}D_{1,i}' + T_{16}D_{0,i}' + T_{17}N_i + T_{18}M_i + \int_{-l}^{l}\frac{N'(\xi)}{x_i - \xi}\,\mathrm{d}\xi$$
$$= \frac{\pi Y^{(s)}}{2(1 - \nu^{(s)^2})}\left(\varepsilon_x^{\infty} + \frac{\phi_{bt}b_{31}}{h\delta_{33}}\right), \tag{16}$$

$$T_{21}N_i'''' + T_{22}M_i'''' + T_{23}N_i'' + T_{24}M_i'' + T_{25}D_{0,i}' + T_{26}M_i + \int_{-l}^{l} \frac{hN''(\xi) - 2M''(\xi)}{(x_i - \xi)^2}\,\mathrm{d}\xi = 0, \tag{17}$$

whereas the governing equations (3) and (4) could be satisfied at the $(n-1)$ discrete points x_i $(i = 1, 2, \ldots, n-1)$ within the interval of $(-l, l)$, i.e.

$$\delta_{11}hD_{0,i} - \frac{h^3\delta_{33}}{12}D_{0,i}'' - (b_{15} + b_{31})M_i' + \frac{b_{15}h}{2}N_i' + \frac{b_{33}h^2}{10}M_i'' - \frac{b_{33}h^3}{24}N_i''' = 0, \tag{18}$$

$$-120\delta_{11}D_{1,i} + 2h^2\delta_{33}D_{1,i}'' - 60b_{15}N_i' + h^2b_{33}N_i''' = 0. \tag{19}$$

Involved in the governing equations are not only the high-order derivatives but also integrals with the strongly singular kernels. The derivatives in the system of integro-differential equations are approximated by the conventional finite difference scheme (Appendix A). The integral in Eq. (8b), in which the integrand, the axial force N, is bounded, could be approximated by using the Trapezium rule with a local error $O(t^2)$, i.e.

$$\int_{-l}^{l} N(\xi)\,\mathrm{d}\xi = t\sum_{j=1}^{n-1} N_j. \tag{20}$$

The two integrals with singular kernels in Eqs. (16) and (17) cannot be approximated by directly using the standard quadrature algorithm. Weakening of the singularity of the integrands would be helpful for achieving an accurate numerical quadrature. This can be realized by using the technique of Kaya and Erdogan (1987) that evaluates integrals having a strongly singular kernel. It can be proved that

$$\int_{-l}^{l} \frac{N'(\xi)}{x_i - \xi}\,\mathrm{d}\xi = -\int_{-l}^{l} \frac{N_i' - N'(\xi)}{x_i - \xi}\,\mathrm{d}\xi + N_i' \ln\left(\frac{l + x_i}{l - x_i}\right), \tag{21}$$

$$\begin{aligned}
&\int_{-l}^{l} \frac{-2M''(\xi) + hN''(\xi)}{(x_i - \xi)^2}\,\mathrm{d}\xi \\
&\quad = \int_{-l}^{l} \frac{(-2M''(\xi) + hN''(\xi)) - (-2M_i'' + hN_i'') - (\xi - x_i)(-2M_i'''' + hN_i'''')}{(x_i - \xi)^2}\,\mathrm{d}\xi \\
&\qquad + (-2M_i'' + hN_i'')\frac{2l}{x_i^2 - l^2} + (-2M_i'''' + hN_i'''')\ln\left(\frac{l - x_i}{l + x_i}\right).
\end{aligned} \tag{22}$$

The integrands of the integrals at the right-hand side of Eqs. (21) and (22) approach to $N''(x_i)$ and $-2M''''(x_i) + hN''''(x_i)$, respectively, as $\xi \to x_i$, which are finite when $i = 1, 2, \ldots, n-1$. Such integrals may, then, be approximated by such a numerical quadrature method as trapezium rule with a local error $O(t^2)$, i.e.

$$\int_{-l}^{l} \frac{N'(\xi)}{x_i - \xi}\,\mathrm{d}\xi = -t\left[\frac{x_iN_i'}{x_i^2 - l^2} + \sum_{j=1, j\neq i}^{n-1} \frac{N_i' - N_j'}{x_i - x_j} + N_i''\right] + N_i' \ln\left(\frac{l + x_i}{l - x_i}\right), \tag{23}$$

$$\begin{aligned}
&\int_{-l}^{l} \frac{-2M''(\xi) + hN''(\xi)}{(x_i - \xi)^2}\,\mathrm{d}\xi \\
&\quad = \frac{t}{2}\left\{\frac{1}{(x_i + l)^2}[(-2M_0'' + hN_0'') - (-2M_i'' + hN_i'') + (l + x_i)(-2M_i'''' + hN_i'''')]\right. \\
&\qquad \left. + 2\sum_{j=1, j\neq i}^{n-1} \frac{1}{(x_i - x_j)^2}[(-2M_j'' + hN_j'') - (-2M_i'' + hN_i'') + (x_i - x_j)(-2M_i'''' + hN_i'''')]\right.
\end{aligned}$$

$$+\frac{1}{(x_i-l)^2}\left[(-2M_n''+hN_n'')-(-2M_i''+hN_i'')-(l-x_i)(-2M_i'''+hN_i''')\right]+(-2M_i''''+hN_i'''')\Bigg\}$$
$$+(-2M_i''+hN_i'')\frac{2l}{x_i^2-l^2}+(-2M_i'''+hN_i''')\ln\left(\frac{l-x_i}{l+x_i}\right). \tag{24}$$

By using the finite difference scheme given in Appendix A, Eqs. (10a)–(19) will result in $4n+4$ algebra equations in terms of values of M, N, D_0 and D_1, at the $(n+1)$ discrete points x_i, $(i=0,1,2,\ldots,n)$ as follows:

$$\sum_{i=0}^{n}K_{1i}^{(k)}D_{0,i}+\sum_{i=0}^{n}K_{2i}^{(k)}D_{1,i}+\sum_{i=0}^{n}K_{3i}^{(k)}N_i+\sum_{i=0}^{n}K_{4i}^{(k)}M_i=C^{(k)},\quad k=1,\ldots,4n+4. \tag{25}$$

where the coefficients $K_{1i}^{(k)}$, $K_{2i}^{(k)}$, $K_{3i}^{(k)}$, $K_{4i}^{(k)}$ and $C^{(k)}$ are constants. They are functions of the material constants, the geometry parameters, the number of discrete points n and the supplied voltage for an actuator (or the substrate strain for a sensor). Explicit expressions for them seem very cumbersome and are unnecessarily to be given out. However the coefficient constants can be easily computed via a computer program. It is expected that the numerical solution approaches the exact solution as the number of points n takes on larger and larger values. Without difficulty the stress fields and electric quantities can be evaluated by substituting the solutions for M, N, D_0 and D_1, into the numerical form of the respective formulae derived in Part I.

3. Convergence of the algorithm

Assume that a PZT-5H thin layer with poling in z direction is adhered on the surface of a steel half plane. The length and the thickness of the piezoceramic piece are 20 and 0.5 mm, respectively, the Young's modulus of the substrate is 207.0 GPa, Poisson's ratio of the substrate equals to 0.27. The three dimensional material constants of the PZT-5H are given by Qi et al. (2001), which could be transformed into the following plane strain constants (Sosa, 1991),

$$a_{11}=8.44023\times10^{-12}\ \mathrm{m^2/N},\quad a_{13}=-2.1983\times10^{-12}\ \mathrm{m^2/N},\quad a_{33}=6.87134\times10^{-12}\ \mathrm{m^2/N},$$
$$a_{44}=1.83692\times10^{-11}\ \mathrm{m^2/N},\quad b_{31}=-0.00816014\ \mathrm{m^2/C},\quad b_{33}=0.0134147\ \mathrm{m^2/C},$$
$$b_{15}=0.0206805\ \mathrm{m^2/C},\quad \delta_{11}=4.29425\times10^{7}\ \mathrm{V^2/N},\quad \delta_{33}=4.87997\times10^{7}\ \mathrm{V^2/N}.$$

In order to discuss the convergence of the algorithm we assume that the PZT patch is used as a sensor. In this case a uniform transverse strain, $\varepsilon_x^{\infty}=1$, is loaded on the host material while the induced electric potential difference, ϕ_{bt}, given by Eq. (8b) has to be inserted Eq. (16) in order to derive the algebra equation (25). Figs. 1–4 show the distributions of the variables M, N, D_0 and D_1 against the normalized distance x/l, respectively. In order to illustrate the convergence of the solutions with the number of discrete points, n, each figure includes three curves, which are associated with the three different values of the number of discrete points, $n=400$, $n=500$ and $n=600$. It can be seen that the values of M, N, D_0 and D_1 over the whole length of the PZT have tiny changes with an increasing n when the number of discrete points n is larger than 500.

In general the numerical values of the interfacial stresses and the sensor output voltage are not accurate as the values of M, N, D_0 and D_1 because they involve the derivatives of M, N, D_0 and D_1. Therefore the variation of the interfacial stresses and of the sensor output voltage versus the number of discrete points n

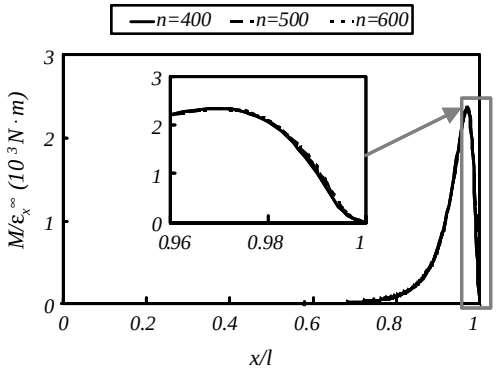

Fig. 1. Convergence of the variable M.

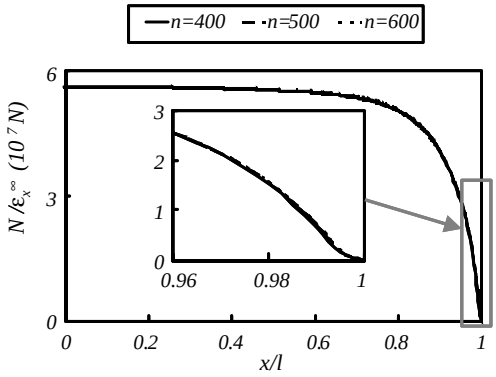

Fig. 2. Convergence of the variable N.

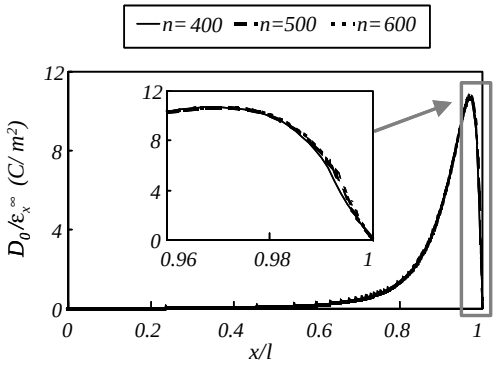

Fig. 3. Convergence of the variable D_0.

should be more critical to enhance confidence in the convergence of the algorithm. Figs. 5 and 6 illustrate the convergence of the interfacial shear and normal stresses, respectively.

Table 1 shows the convergence of the output voltage against the number of discrete points n.

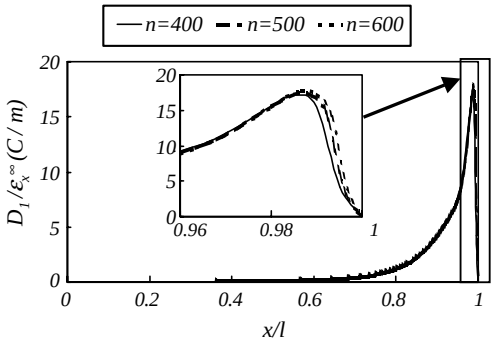

Fig. 4. Convergence of the variable D_1.

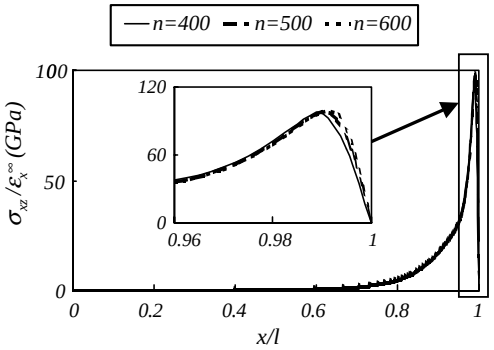

Fig. 5. Convergence of the interfacial shear stress.

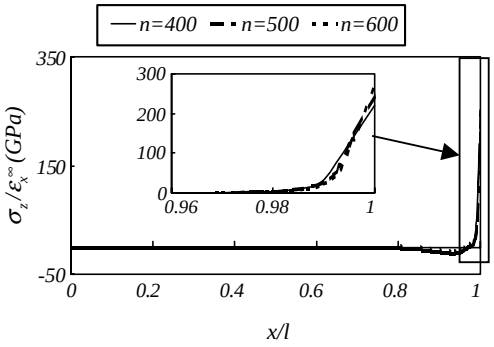

Fig. 6. Convergence of the interfacial normal stress.

It can be seen that the convergence of these variables having higher-order derivatives are comparable with that of the variables M, N, D_0 and D_1. Therefore the convergence of the algorithm is believed to be enough when n is more than 500. We will select $n = 500$ at the following discussions, and the material constants will have the same values as those in this section.

Table 1
Convergence of the output voltage

Discrete points, n	$\phi_{bt}/\varepsilon_x^{\infty}$ (V).
400	-4.2021×10^5
500	-4.2039×10^5
600	-4.2049×10^5

4. Application as an actuator

Assume that the piezoceramic layer acts as an actuator and is coated by the electrodes on the top and bottom surfaces. A unit voltage of $\phi_{bt} = V = 1$ V is supplied to the electrodes while no external mechanical force is imposed on the structure $\varepsilon_x^{\infty} = 0$, Fig. 7.

Fig. 8(a) and (b) is the density and contour plots of the electric field intensity in the x-direction, E_x, respectively. It can be seen that the electric field component, E_x, concentrates near the edges and vanishes in the interior region.

Fig. 9(a) and (b) is the density and contour plots of the electric field intensity in the z-direction, E_z, respectively.

The electric field component E_z is homogeneous in the middle part of the piezoceramic whereas it is distorted near the left and right edges of the piezoceramic layer.

The length of the electric disturbance occupies about one-third of the total length of the PZT. It is caused by the electric boundary condition as well as by the fully electromechanical coupling. It is suggested that a significant error could be caused by the assumption of a uniform electric field which neglects the spatial variation in the piezoceramic layer (Wang and Meguid, 2000).

Fig. 10(a) and (b) is the density and contour plots of the electric potential ϕ, respectively.

The electric potential gets the maximum at the bottom surface and the minimum at the top surface. Obviously, the edge disturbance influences the electric potential not significantly as the electric field intensity.

Fig. 11 shows the distribution of the interfacial stresses versus the normalized distance x/l.

There exists a severe stress concentration near the interface tip. The concentration is believed due to two reasons. One is that the mismatch strain of the PZT induced by the applied voltage is constrained by the elastic substrate. The other is that the inhomogeneous distribution of electric fields in the PZT results in a non-uniform stress distribution via the coupled electromechanical constitutive behavior. The value of the interfacial normal stress is much higher than the value of the interfacial shear stress. This suggests that the interfacial normal stress could be the main cause of the interface debonding initiation.

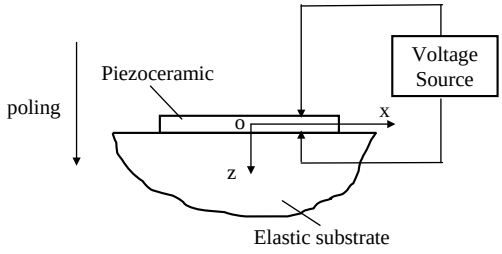

Fig. 7. A piezoelectric actuator bonded to a structure.

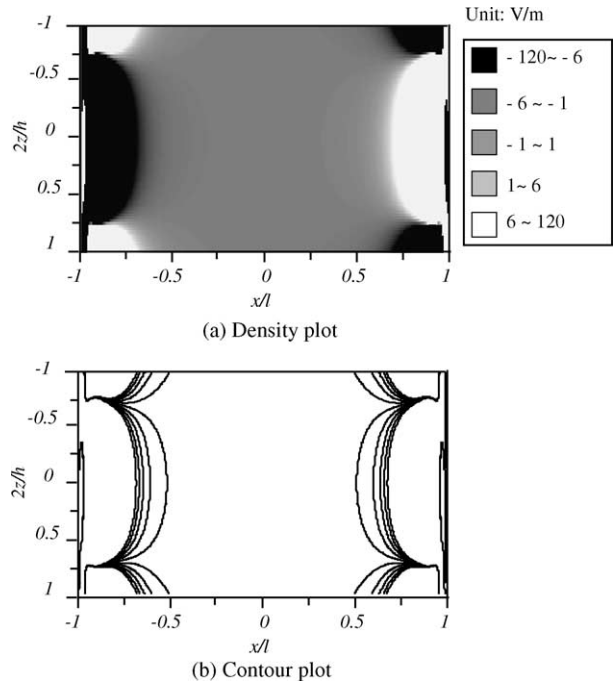

Fig. 8. Distribution of the electric field intensity, E_x, in the piezoceramic actuator: (a) density plot and (b) contour plot.

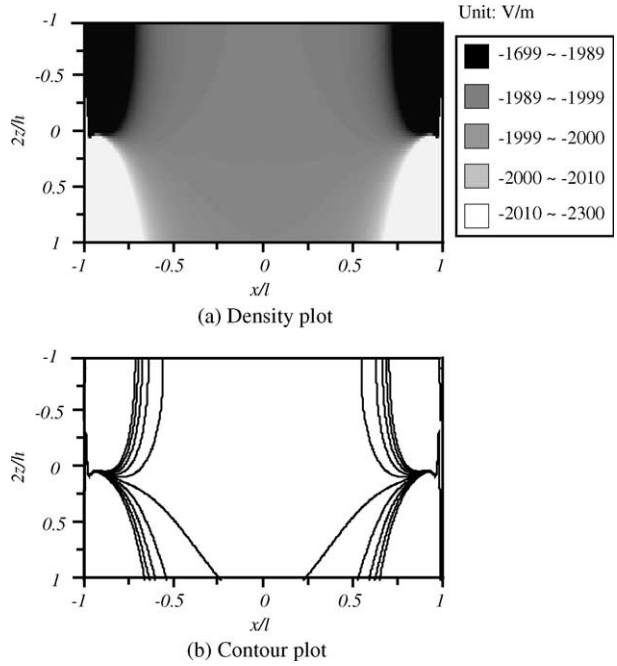

Fig. 9. Distribution of the electric field intensity, E_z, in the piezoceramic actuator: (a) density plot and (b) contour plot.

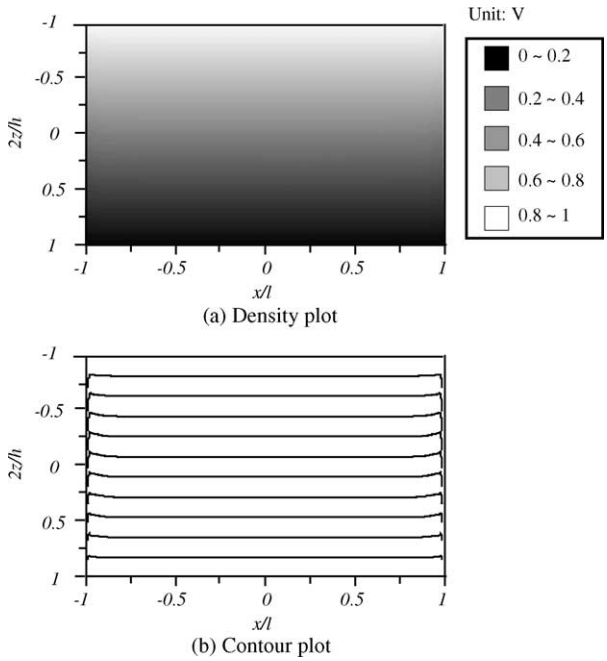

Fig. 10. Distribution of the electric potential, ϕ, in the piezoceramic actuator: (a) density plot and (b) contour plot.

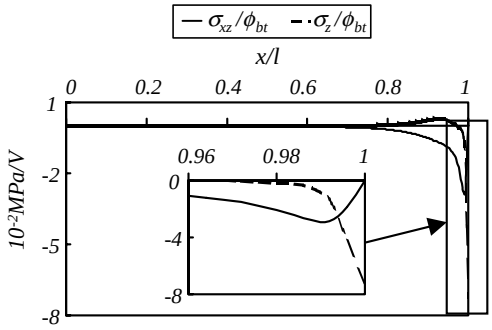

Fig. 11. The interfacial shear and normal stresses when the piezoceramic acts as an actuator.

5. Application as a sensor

In Section 3, we have taken the piezoceramic sensor as an example for the purpose of the examination of the convergence of the numerical algorithm. Here we consider it again in order to examine the electric and mechanical behaviors from the aspect of measuring application. The strain in the substrate ε_x^{∞} transmits to the PZT sensor via the interface, causing an electric field in the layer. Figs. 12 and 13 show the density and contour plots of the electric field components in x- and z- directions, E_x and E_z, respectively.

Fig. 14 is the density and contour plots of the electric potential respectively.

Both the electric field intensity and the electric potential do not vary significantly with the x-coordinate in the middle part while an electric concentration exists near the left and right edges of the piezoceramic layer. The disturbance affects about one-third of the length.

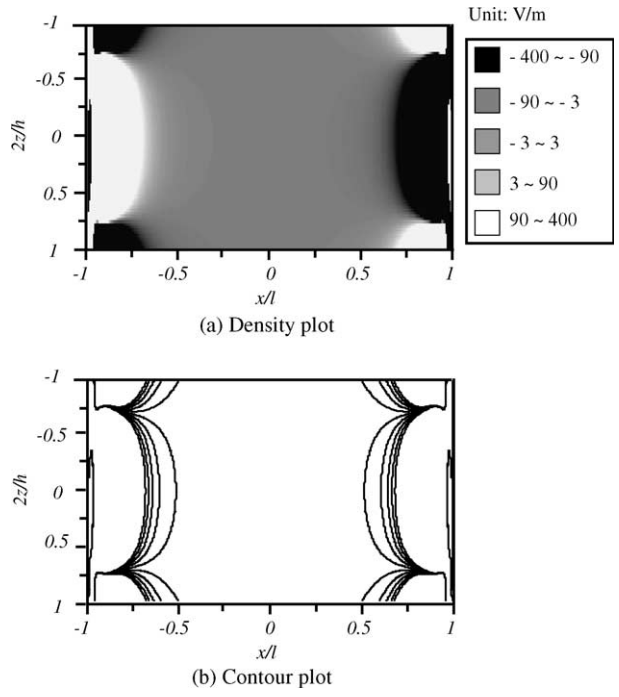

Fig. 12. Distribution of the electric field intensity, E_x, in the piezoceramic sensor induced by $\varepsilon_x^{\infty} = 10^{-6}$: (a) density plot and (b) contour plot.

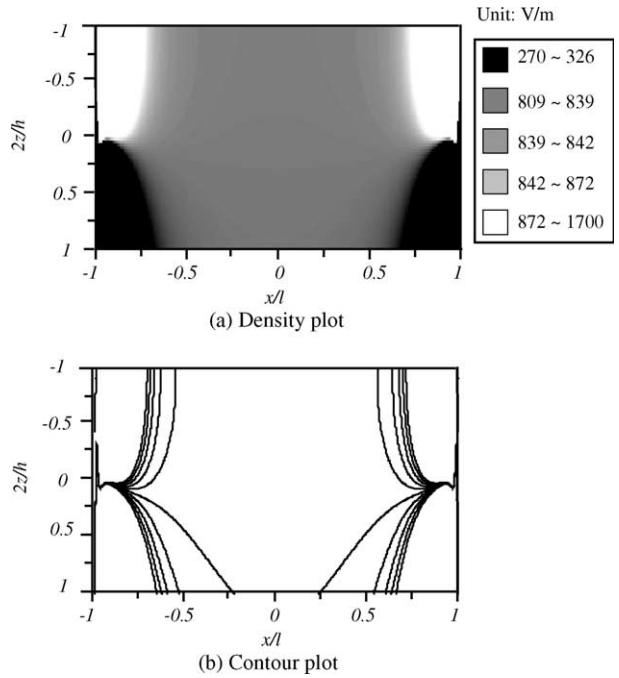

Fig. 13. Distribution of the electric field intensity, E_z, in the piezoceramic sensor induced by $\varepsilon_x^{\infty} = 10^{-6}$: (a) density plot and (b) contour plot.

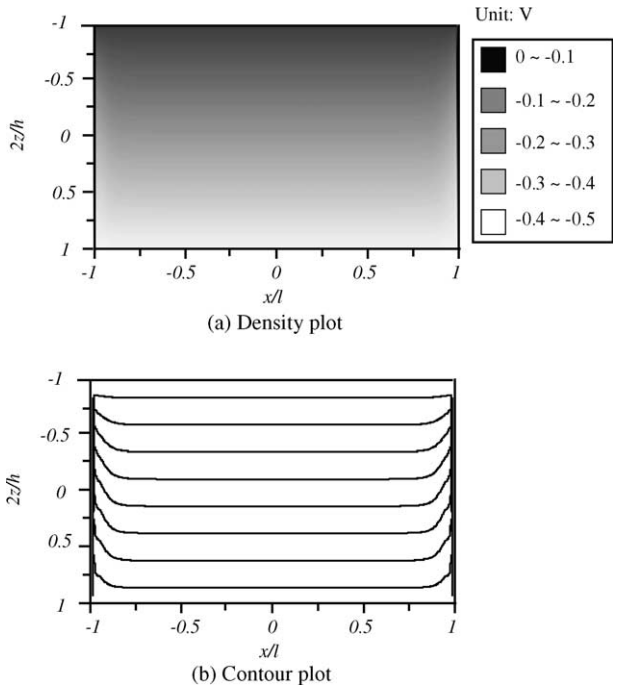

Fig. 14. Distribution of the electric potential, ϕ, in the piezoceramic sensor induced by $\varepsilon_x^{\infty} = 10^{-6}$: (a) density plot and (b) contour plot.

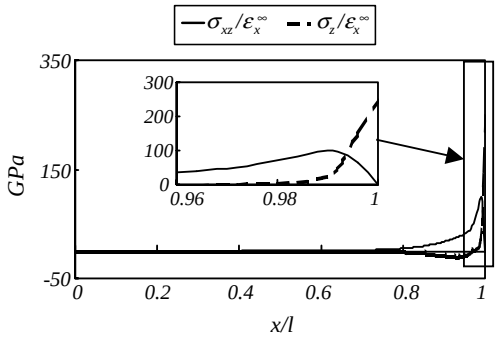

Fig. 15. The interfacial shear and normal stresses when the piezoceramic acts as a sensor.

Fig. 15 illustrates the distribution of the interfacial stresses. The interfacial stress concentration is observed near the tip. Therefore the interfacial normal stress is believed to control the interface delamination initiation.

A quantitative relationship between the substrate strain to be measured and the output voltage would be very useful for calibration of the sensor. Within the linearity domain one may introduce transformation factor as follow:

$$k_t = \frac{\text{Substrate strain}}{\text{Output voltage}} = \frac{\varepsilon_x^{\infty}}{\phi_{bt}}, \quad \varepsilon_x^{\infty} = k_t \phi_{bt}.$$

We have $k_t = 2.38$ ($\mu\varepsilon$/V) in the examined system.

6. Conclusion

In this Part II of the paper, we have proposed a numerical solution algorithm for the governing integro-differential equations presented in Part I to analyze a piezoceramic actuator/sensor adhered on an elastic substrate. There are lots of the real-world problems, which lead to such a form of integro-differential equations. The numerical results show that the proposed algorithm is effective and stable.

The numerical results of the electric fields indicate clearly that the electric field intensity has a significant disturbance near the left and right edges of the piezoelectric layer for both the cases of actuator and sensor. So one cannot assume the electric field intensity to be homogeneous in the whole piezoceramic material. There exists also a spatial gradient of the electric potential near the edges for both the actuator and the sensor. However the magnitude of the electric gradients caused by the edge boundaries is more significant in sensor than that in actuator. The higher electric potential gradient in the sensor is attributed to the spatial variation in the mechanical stresses. For the case of actuator considered, however, the fact that the mechanically induced electric potential is relatively smaller compared to the applied voltage leads to a less spatially varying potential.

The interfacial normal and shear stresses between the piezoceramic layer and the substrate concentrate near the tips. The normal stress, which is much higher than the shear stress, is believed to control the delamination initiation.

Acknowledgements

Authors gratefully acknowledge the financial supports by the Applied Research Foundation of the City of Chongqing, and the National Science Foundation of China under the grant number 59503003.

Appendix A. Finite difference schemes

The finite difference schemes selected for approximating derivatives are summarized with notation $F_i = F(x_i)$ as follows:

$$F_0' = \frac{-F_2 + 4F_1 - 3F_0}{2t},$$

$$F_i' = \frac{F_{i+1} - F_{i-1}}{2t}, \quad i = 1, 2, \ldots, n-1,$$

$$F_n' = \frac{-F_{n-2} + 4F_{n-1} - 3F_n}{2t},$$

$$F_0'' = \frac{2F_0 - 5F_1 + 4F_2 - F_3}{t^2},$$

$$F_i'' = \frac{F_{i+1} - 2F_i + F_{i-1}}{t^2}, \quad i = 1, 2, \ldots, n-1,$$

$$F_n'' = \frac{2F_n - 5F_{n-1} + 4F_{n-2} - F_{n-3}}{t^2},$$

$$F_1''' = \frac{20F_1 - 6F_0 - 24F_2 + 12F_3 - 2F_4}{4t^3},$$

$$F_i''' = \frac{F_{i+2} - 2F_{i+1} + 2F_{i-1} - F_{i-2}}{2t^3}, \quad i = 2, 3, \ldots, n-2,$$

$$F_{n-1}''' = \frac{20F_{n-1} - 6F_n - 24F_{n-2} + 12F_{n-3} - 2F_{n-4}}{4t^3},$$

$$F_i'''' = \frac{F_{i+2} - 4F_{i+1} + 6F_i - 4F_{i-1} + F_{i-2}}{t^4}, \quad i = 2, 3, \ldots, n-2,$$

where F could be any one of M, N, D_0 and D_1. Each finite difference scheme has a local error of $O(t^2)$.

References

Benes, E., Gröschl, M., Burger, W., Schmid, M., 1995. Sensors based on piezoelectric resonators. Sensors and Actuators A 48, 1–21.

Bland, S.R., 1970. The two-dimensional oscillating airfoil in a wind tunnel in subsonic flow. SIAM Journal of Applied Mathematics 18, 830–848.

Cess, R.D., Tiwari, S.N., 1969. The interaction of thermal conduction and infrared gaseous radiation. Applied Science Research 20, 25–39.

Delves, L.M., Walsh, J., 1974. Numerical Solution of Integral Equations. Clarendon Press, Oxford.

Dragos, L., 1990. Numerical solution of the equation for a thin airfoil in ground effect. AIAA Journal 28, 2132–2134.

Erdogan, F., Gupta, G.D., 1972. On the numerical solution of singular integral equations. Quarterly of Applied Mathematics 30, 525–534.

Frankel, J.I., 1995. A Galerkin solution to a regularized Cauchy singular integro-differential equation. Quarterly of Applied Mathematics 53 (2), 245–258.

Kaya, A.C., Erdogan, F., 1987. On the solution of integral equations with strongly singular kernels. Quarterly of Applied Mathematics 45 (1), 105–122.

Lapidus, L., Pinder, G.F., 1982. Numerical Solution of Partial Differential Equations in Science and Engineering. John Wiley & Sons, New York.

Li, L.K., Yu, C.H., Zhu, Z.H., 1999. Numerical Solution of Differential Equations. Fudan University Press, Shanghai (in Chinese).

Loakimidis, N.I., 1983. Further convergence results for the weighted Galerkin algorithm of numerical solution of Cauchy-type singular integral equations. Mathematics of Computation 41 (163), 79–85.

Muskhelishvili, N.I., 1953. Singular Integral Equations. P. Noordhoff LTD, Groningen, Holland.

Pal, P.F., Rommei, B., Schulz, M.J., 2000. Dynamics regulation of a skew cantilever plate using PZT patched and saturation phenomenon. Journal of Intelligent Material Systems and Structures 11, 642–655.

Plotkin, A., Dodbele, S.S., 1988. Slender wing in ground effect. AIAA Journal 26, 493–494.

Qi, H., Fang, D.N., Yao, Z.H., 2001. Analysis of electric boundary condition effects on crack propagation in piezoelectric ceramics. Acta Mechanica Sinica (English series) 17 (1), 59–70.

Sankar, T.S., Hoa, S.V., Fabrikant, V.I., 1982. Approximate solution of singular integro-differential equations in elastic contact problems. International Journal for Numerical Methods In Engineering 18 (4), 503–519.

Sosa, H., 1991. Plane problems in piezoelectric media with defects. International Journal Solids Structure 28, 491–505.

Styś, K., Styś, T., 2000. A higher-order finite difference algorithm for solving a system of integro-differential equations. Journal of Computational and Applied Mathematics 126, 33–46.

Wang, B.T., Chen, R.L., 2000. The use of piezoceramic transducers for smart structural testing. Journal of Intelligent Material Systems and Structures 11, 713–724.

Wang, X.D., Meguid, S.A., 2000. On the electroelastic behaviour of a thin piezoelectric actuator attached to an infinite host structure. International Journal of Solids and Structures 37, 3231–3251.